InAs/GaAs(001) epitaxy: kinetic effects in the two-dimensional to three-dimensional transition

2007 J. Phys.: Condens. Matter 19 225006

(http://iopscience.iop.org/0953-8984/19/22/225006)

IOP PUBLISHING JOURNAL OF PHYSICS: CONDENSED MATTER

J. Phys.: Condens. Matter **19** (2007) 225006 (21pp) doi:10.1088/0953-8984/19/22/225006

InAs/GaAs(001) epitaxy: kinetic effects in the two-dimensional to three-dimensional transition

E Placidi[1,3], F Arciprete[2], M Fanfoni[2], F Patella[2], E Orsini[2] and A Balzarotti[2]

[1] CNR-INFM, Via della Ricerca Scientifica 1, I-00133 Roma, Italy
[2] Dipartimento di Fisica, Università di Roma 'Tor Vergata', Via della Ricerca Scientifica 1, I-00133 Roma, Italy

E-mail: ernesto.placidi@roma2.infn.it

Received 28 September 2006
Published 14 May 2007
Online at stacks.iop.org/JPhysCM/19/225006

Abstract

Step instability and surface mass transport strongly influence the kinetics of the two- to three-dimensional (2D–3D) transition in InAs/GaAs self-assembly epitaxy. In this paper we report evidence of the step erosion of quantum dots (QDs) nucleated on step edges for samples having different surface morphologies and the explosive nucleation of 3D QDs triggered by it. Related issues such as the temperature dependence of the critical thickness, the volume dependence of the surface mass transport, and the scaling behaviour are illustrated by means of RHEED and AFM measurements and data analysis for small increments of InAs coverage throughout the 2D–3D transition.

(Some figures in this article are in colour only in the electronic version)

1. Introduction

Heteroepitaxy is defined as the growth of a crystalline film (element or compound) reproducing the surface order of a different crystalline substrate, either lattice matched or lattice mismatched with the film being deposited. In this process, the lowering of the excess surface free energy leads to three types of macroscopic growth named (i) Frank–Van der Merwe, i.e. the two-dimensional (2D) layer-by-layer growth, (ii) Volmer–Weber, i.e. the formation of three-dimensional (3D) islands of the deposited material directly on the substrate, and (iii) Stranski–Krastanow, i.e. the growth of a 2D wetting layer of the material being deposited up to a critical thickness, followed by the transition to 3D island growth.

The latter growth mode—considered as an undesirable feature in strained heteroepitaxy of quantum well systems—gained much attention, from the 1990s onward, when it was discovered that, at the initial stage of the 3D growth, a narrow size distribution in height and lateral

[3] Author to whom any correspondence should be addressed.

dimension of small coherent islands (defect free) formed. It was soon clear that quantum confinement effects, i.e. the quasi-zero-dimensional density of states of such islands—termed 'quantum dots (QDs)' —could be used to realize devices with improved optical properties with respect to those based on strained III–V superlattices, as for the case of InAs QDs on GaAs.

In heteroepitaxy of InAs/GaAs(001), the strained growing layer remains planar up to a characteristic coverage (critical thickness), above which three-dimensional (3D) islands form. Such a growth mode transition is the most distinctive aspect of the InAs/GaAs(001) system and is at the basis of the formation of self-assembled quantum dots. Although of the Stranski–Krastanov type, such a transition has a more complex evolution from its initial stage. Specific issues which differ from the conventional Stranski–Krastanov growth are, for instance, the following:

(i) the 2D wetting layer (WL) is an InGaAs alloy having a precise composition at the transition [1–3];

(ii) the 2D to 3D transition, at the critical thickness, occurs within 0.2 ML of InAs deposition, by the sudden nucleation of 10^{10}–10^{11} cm^{-2} QDs which are coherent and strained;

(iii) InAs QDs include some Ga at their bases, whose amount depends on growth conditions;

(iv) the nucleated 3D volume is far larger than that being deposited in the narrow coverage range where nucleation is completed.

Other details of InAs/GaAs heteroepitaxy concern thermodynamic and kinetic aspects of the growth, such as the dependence of the critical thickness on substrate temperature and In flux, which is unexpectedly weak according to kinetics.

The interesting perspectives of QDs for optoelectronic devices, quantum computing and quantum cryptography drove much attention on other important issues affecting the optical performance of self-assembled QDs. These are the homogeneity of their size and shape and the correlation of their lateral position on the surface. The fabrication of ordered arrays of dots by epitaxy, minimizing lithographic processes, would be highly advantageous for optoelectronic applications. This, however, requires first the comprehension and then the capability to control at the nanoscale microscopic processes involved in the 2D–3D transition. The issues listed above are among those lacking, at present, a sufficient understanding, with reference, in particular, to the dependence on substrate morphology, surface stress and kinetics of growth [4–7].

Having in mind this research perspective, we reported here the main results of our studies on the InAs/GaAs(001) heterostructure aiming at the investigation of the basic microscopic mechanisms driving the nucleation of QDs at each stage of their evolution. The experimental approach adopted was to grow the InAs/GaAs interface using different molecular beam epitaxy (MBE) procedures, and to examine its surface morphology by atomic force microscopy (AFM) and reflection high energy electron diffraction (RHEED). Thus, experimental size distributions, volume and number density of dots, kinetics and scaling properties for different morphological conditions were comparatively analysed for very small increments of InAs coverage throughout the 2D–3D transition. The strategy for tracing the evolution of 2D–3D transition in great experimental detail is to obtain, on a 2 inch long sample, the entire transition at once from the WL to QDs. How this is achieved is explained in the section 2, where are briefly described also the growth procedures and characterization techniques utilized in these studies. The main results are discussed in the following sections, also in relation to other experimental and well established theoretical data present in the current literature [8, 9].

2. Heteroepitaxial growth of InAs on GaAs(001)

2.1. Sample preparation and characterization techniques

In two independent MBE growths, the same film thickness can be obtained, typically within ± 0.05 ML, because of unavoidable small fluctuations of the beam fluxes, sample temperature etc. Furthermore, the angular dependence of the Knudsen-cell flux at the position of the substrate produces, in principle, a thickness gradient on large samples. Nonetheless, thickness uniformity can be obtained on substrates up to 3 inches, since in standard growth any angular dependence is averaged by rotating the substrate. In contrast, in the case of a non-rotating substrate, the growth velocity increases linearly and the rate can be accurately measured by RHEED oscillations. In this last case, one can take advantage of the angular distribution of the flux to overcome problems of reproducibility in achieving thickness differences as small as ± 0.01 ML, because the range of thickness widens simultaneously. For InAs on GaAs(001), such a procedure was adopted to obtain the full 2D–3D transition on the same surface. Thus, the structural evolution of InAs QDs, occurring within 0.2 ML above the critical thickness [10–14], is studied for coverage increments of ± 0.01 ML in the range 0.9–2.2 ML.

Three samples were prepared using different MBE procedures. In the first sample, labelled 'GI', the In delivery was cycled in 5 s of evaporation followed by 25 s of growth interruption (GI) (with the As shutter always left open) until the onset of the 2D–3D transition was observed by RHEED at the centre of the sample [14]. The second sample, labelled as 'GI-flat', was grown with the same procedure on a GaAs(001) surface flattened by a 80 min post-growth annealing at 660 °C under As_4 flux [15]. The third one, labelled 'CG', was grown in the continuous growth (CG) mode, i.e. by delivering In for 80 s on a standard GaAs(001) buffer.

Prior to InAs deposition, a GaAs regrowth of approximately 500 nm at 590 °C was performed on the (001)-oriented substrate, in As_4 overflow, at a rate of 1 μm h^{-1}. After 10 min post-growth annealing the temperature was lowered to 500 °C, when a GaAs c(4 × 4) surface was observed. The InAs growth was carried out without rotating the substrate, so as to obtain the aforementioned thickness profile along the sample. As illustrated in figure 1, the sample was placed in region (b) where the impinging flux increased linearly along the [110] direction of the substrate, from 0.011 to 0.030 ML s^{-1}, resulting in InAs coverages ranging from 0.87 to 2.40 ML for 80 s of growth. The growth velocity was measured by RHEED intensity oscillations at various points of the GaAs substrate along the [110] direction.

The structural characterization of the three samples, on a set of points along the [110] direction, was performed by atomic force microscopy (VEECO Multiprobe), in air, in the tapping mode and with non-conductive Si tips.

In order to investigate the effect of temperature around the critical thickness, other two sets of InAs/GaAs(001) samples were grown, both in the CG and in the GI mode, for a fixed InAs coverage of approximately 2.2 ML and substrate temperatures ranging from 450 to 560 °C. The spotty RHEED patterns signal the formation of QDs (figure 2). The RHEED intensity was monitored by a CCD camera. The steep rise in the intensity occurring marks the 2D–3D onset at the coverage θ_c, the critical thickness for the 2D–3D transition.

The growth velocity of InAs, V_{InAs}, is a function of the substrate temperature, and was calibrated by means of RHEED intensity oscillations. The RHEED oscillations are clearly detected on As-rich InAs(001) surface reconstructions, which are stable in a very narrow range of growth parameters and temperatures. In order to expand the measure of V_{InAs} in the entire temperature range of interest, we proceeded as follows. The beam fluxes of Ga, In and As were chosen and remained the same for all growths. First, the GaAs on GaAs(001) growth rate, V_{GaAs}, was measured by RHEED oscillations in the substrate temperature range 450–600 °C.

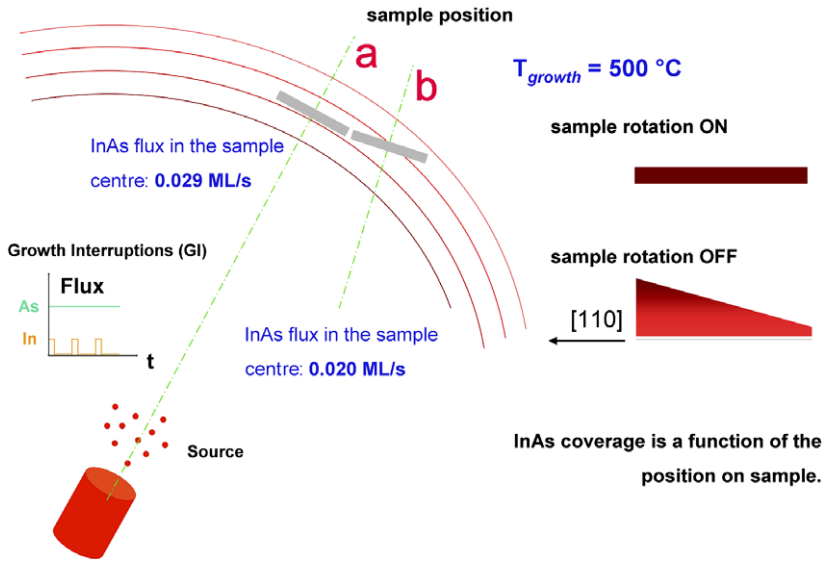

Figure 1. Schematic diagram of the growth geometry in the MBE reactor. In the standard sample position (a) the flux wave front is nearly parallel to the surface while at oblique incidence (b) a coverage gradient is present.

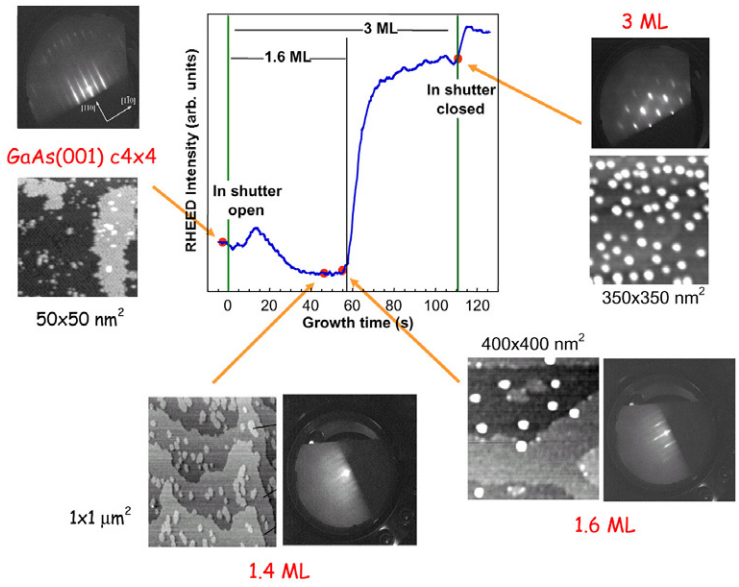

Figure 2. The graph represents the 2D–3D transition monitored by the RHEED intensity. RHEED patterns, STM (c(4 × 4) reconstruction) and AFM images are shown for significant coverages.

Independently of the initial c(4 × 4) or (2 × 4) As-rich GaAs(001) reconstructions, such a rate was 0.0834 ML s^{-1}, and was constant within 0.0002 ML s^{-1}. Then, we measured the growth rate, V_{InGaAs}, of a diluted $In_xGa_{1-x}As$ alloy on GaAs(001) at all the temperatures in the range 450–560 °C (the starting concentration, $x \leqslant 0.25$ at 450 °C, was sufficiently low to maintain

Table 1. Growth rate, V_{InAs}, of InAs on GaAs(001) and its percentage decrease, $(\Delta V/V)_{\mathrm{InAs}}$, in the temperature range 450–560 °C.

	450–500 °C	520 °C	530 °C	535 °C	545 °C	560 °C
V_{InGaAs} (ML s^{-1})	0.1125	0.1120	0.1115	0.1108	0.1094	0.1083
V_{InAs} (ML s^{-1})	0.0291	0.0286	0.0280	0.0274	0.0260	0.0249
$(\Delta V/V)_{\mathrm{InAs}}$	0	1.8%	3.6%	5.7%	10.8%	14.3%

the 2D growth). This rate was constant up to approximately 500 °C and decreased above: i.e., the time required for depositing one monolayer of alloy increased above 500 °C. Such a time, in III–V MBE growth, is determined solely by the adsorption rate of the element III. It follows that a diminished amount of group-III species was adsorbed on the alloy surface at temperatures higher than 500 °C, for equal evaporation times and constant In and Ga fluxes. The growth velocity V_{InGaAs} is related to V_{InAs} and V_{GaAs} by the MBE growth-velocity equation for alloys: $V_{\mathrm{InGaAs}} = V_{\mathrm{InAs}} + V_{\mathrm{GaAs}}$. Since V_{GaAs} was constant in the measured temperature range, any variation of V_{InGaAs} was exclusively due to V_{InAs}. Accordingly, we obtained the growth rates as a function of temperature shown in table 1. The accuracy of the alloy growth equation was independently confirmed by obtaining, within 0.0002 ML s^{-1}, the same V_{InAs} value as reported in table 1, from the RHEED oscillations of InAs on InAs(001) at $T = 500$ °C. V_{InGaAs} (with $x = 0.25$ at 450 °C) and V_{GaAs} were measured by RHEED oscillations as a function of temperature, in the range 450–560 °C, for constant In and Ga fluxes. The measured GaAs growth rate, $V_{\mathrm{GaAs}} = 0.0834$ ML s^{-1}, did not vary in the entire temperature range.

2.2. The 2D phase: wetting layer and critical thickness

Many experimental works in literature report on In segregation and In–Ga intermixing in epitaxial ternary III–V alloys. Among group III elements, In has the highest segregation coefficient, leading to the formation of a quasi-binary surface in ternary alloys. Moison *et al* [16] have estimated, by x-ray photoemission and Auger measurements on the $In_{0.2}Ga_{0.8}As$ bulk compound grown at 480 °C, an average surface In composition of 0.7. Experimental evidence comes also from the observation, by scanning tunnelling microscopy, of the surface reconstructions typical of In-rich InGaAs alloys.

Dehaese, Wallart and Mollot (DWM) [17] proposed a simple kinetic model to treat the segregation process far from equilibrium. In fact, thermodynamic equilibrium models fail in predicting the concentration profiles at high fluxes and low growth temperatures. Because of the very low bulk diffusion coefficient at the typical MBE growth temperatures, the DWM model rests on the hypothesis that the exchange between atoms A and B of a pseudobinary $A_{1-x}B_xC$ alloy takes place solely between the two topmost layers; namely, the growing layer and the layer just below.

A recent significant result is due to Cullis *et al* [1–3]. They propose a model for the Stranski–Krastanov growth of strained semiconductor heterostructures which focuses on the wetting layer (WL) composition and, in particular, on the strain dependence of the critical thickness, in $In_xGa_{1-x}As/GaAs$ systems, as a consequence of In segregation in the WL. The model (called WCNH) is supported by transmission electron microscopy (TEM) measurements of the chemical composition of WL and 3D islands. The data indicate that the 2D–3D transition is triggered by a critical value of the strain as soon as the In concentration of the top surface of the WL reaches a precise value. Around islands the In concentration is found to be lower than the nominal value of the evaporated alloy; meanwhile, it is considerably higher inside the islands. This finding was attributed to the vertical segregation of In, whose concentration in

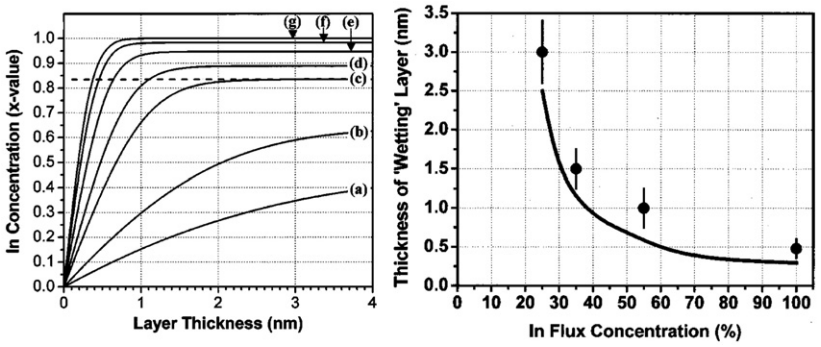

Figure 3. Left panel: composition variations in the surface monolayer, driven by In segregation to the surface, for deposition fluxes with (a) 5% In, (b) 10% In, (c) 25% In, (d) 35% In, (e) 55% In, (f) 80% In, and (g) 100% In. Right panel: variation in the flat-layer critical thickness for the islanding transition as a function of In concentration in the deposition flux: measured values given as data points and theoretically predicted values based upon the WCNH mechanism presented as a continuous curve. Reprinted with permission from [1]. Copyright (2002) by the American Physical Society.

3D islands is higher at the apex, where the lattice parameter is closer to that of bulk InAs. The WCNH mechanism has been simulated using the Fukatsu–Dehase model [18] for In segregation. In this model, segregation continuously raises the In concentration in the top layer to a saturation value (left panel of figure 3), which increases with the nominal In concentration, x, of the alloy. Since $x = 0.25$ is the minimum value for islanding to occur (right panel of figure 3), the saturation concentration of the curve (c) has been identified as the critical one. Thus the 2D–3D transition occurs only when an In concentration of 80–85% is reached.

Tu and Tersoff [19] proposed a continuum model of the heteroepitaxy of Ge/Si and InAs/GaAs alloys that confirm the model of Cullis *et al*. In this model, they do not search for a 2D–3D transition in the literal sense, but they rather find a kinetic crossover to the instability regime of an initially small height-perturbation of the surface, due to the continuous increase of surface In (Ge) content (hence of stress), as shown in figure 4. Furthermore they point out that, while the initial planar growth occurs due to intermixing of deposited material with the substrate, the transition is strictly kinetic in nature and the finite stiffness (steps) and surface mass diffusion are essential ingredients for the instability to set up.

2.3. The 3D phase: evolution of the surface morphology during the 2D–3D transition

As reported in several papers [10, 12–14, 20–22], close to the critical thickness, the morphology of the InAs/GaAs(001) interface becomes quite rich. Figure 5 shows significant AFM topographies (1 μm $\times$ 1 μm) for coverages between 1.42 and 1.60 ML for the samples CG, GI and GI-flat. The images reveal an involved morphology of the WL comprising 2D islands 1 ML high, and large terraces one step high. The three samples are characterized by different initial morphologies of the WL. While in the GI and CG samples, at coverages of 1.42 ML, the AFM topographies reveal a stepped surface, in the GI-flat just a few steps per μm^2 area result from the flattening process (section 2.1) [15]. The morphological instabilities (mounds) of the GI sample are typical of GaAs(001) growth [23]. Indeed, kinetic instabilities of the growth, due to the anisotropy of diffusion and the extra barrier for down-hopping at step edges [24, 25], give rise to the stepped texture of the WL, which strongly influences the in-plane position of dots; in fact, most of them nucleate at step edges [10, 20, 21, 26, 27]. 2D islands appear in all

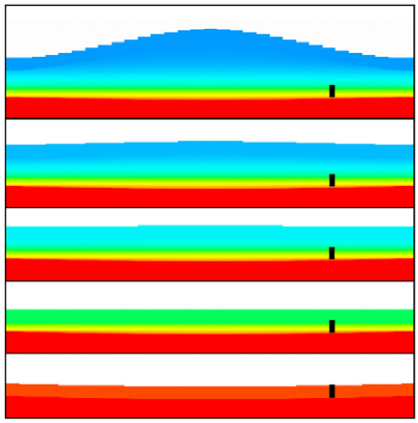

Figure 4. Evolution of structure and composition during heteroepitaxy, for nominal $Si_{0.60}Ge_{0.40}$ on Si(001), at deposition rate of 10^4 (arbitrary units). The onset of nonplanar morphology is more abrupt at lower growth rates. Colours (greyscales) indicate composition, from pure Si substrate (bottom) to $Si_{0.62}Ge_{0.38}$ (top). The bottom panel is the initial surface (slightly nonplanar), and subsequent panels are at equal time intervals. The figure shows one unit cell of the periodic system; the lateral size is 640 w_s. Surface-layer thickness w_s is indicated by a black rectangle in the bottom panel; the vertical scale is greatly expanded to show the small perturbation. The rectangle is repeated in the same position in subsequent panels for reference. Surface steps are a graphical artifact. Reprinted with permission from [19]. Copyright (2004) by the American Physical Society.

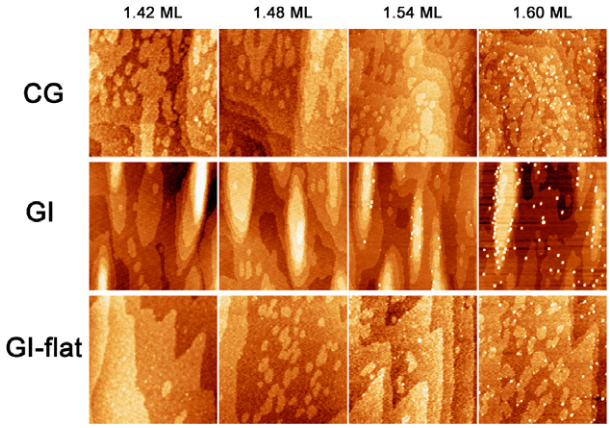

Figure 5. $1 \times 1\ \mu m^2$ AFM topographies for the CG, GI and GI-flat samples. The images show the WL at 1.42 ML, free from 3D features, the first small QDs at 1.48 ML and the occurrence of large QDs at 1.54 ML for the GI sample and at 1.60 ML for the others.

samples at about 1.4 ML and vanish when the massive nucleation of large QDs is taking place. The first small QDs (present in all images) are recognizable for coverage as high as 1.45 ML, whereas at higher InAs deposits (starting from 1.54 ML) the formation and subsequent number increase of large QDs can be seen. Small QDs nucleate preferentially at the upper-step edges of 2D islands and terraces by reason of a favourable strain condition at these sites. They have been reported several times [12, 13, 20–22] and often been indicated as simple precursors of large QDs. However, this simplified picture is unrealistic and we will show in the following sections that the process involves a more complex kinetic mechanism.

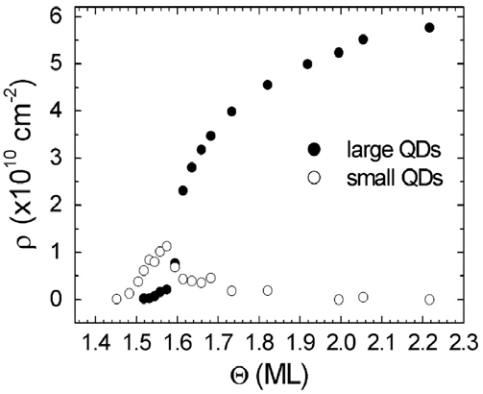

Figure 6. Number density dependence on InAs coverage of small and large QDs.

The number density evolution of both small and large QDs for the CI sample is summarized in figure 6 as a function of InAs deposition. The number of the small QDs begins to increase at 1.45 ML of InAs deposit and maximizes at 1.57 ML, reaching the value of 1.1×10^{10} cm^{-2}. Starting from 1.52 ML, the number of the large QDs increases gradually, then, between 1.57 and 1.61 ML, it undergoes a sudden rise, changing value by an order of magnitude. At higher coverages (>1.8 ML) the density rise is much slower. In this region the density is of the order of 6×10^{10} cm^{-2} for all the samples. The steady increase observable for coverages higher than 1.8 ML is due to the dependence of the density saturation value on growth rate. As shown by theoretical [28, 29] and experimental [30] works, the dependence of the saturation 3D island number density, prior to coalescence, in the complete condensation regime is $N_S \propto F^{i/(i+2.5)}\, \mathrm{e}^{E_\mathrm{a}/k_\mathrm{B}T}$, where F is the flux, E_a is the activation energy for diffusion given by $(E_i - \mathrm{i}E_d)/(i + 2.5)$, E_i is the binding energy of a critical nucleus size i, E_d the diffusion energy and k_B is Boltzmann's constant. The linear increase observed on our sample is in good agreement with results shown by Krzyzewski *et al* [30].

In figure 7 the density of small (left panel) and large QDs (right panel) is shown, by dividing QDs placed on step bunching (crosses) and elsewhere (squares). While for the small QDs the two distributions match, for large QDs the nucleation takes place early by a small coverage, estimated to be 0.03 ML at the middle height of the two distributions. In fact, between 1.55 and 1.75 ML, the nucleation on the step bunching is enhanced compared to that on other regions of the surface. The same is true for the volume increase of QDs (not shown). This is also corroborated by the comparison of surface morphologies at 1.54 ML for the different WLs: as shown in the right panel in figure 7, only when step bunching is present (GI sample) is nucleation of large QDs observed. On the other hand the density of small QDs is not affected by the different strain due to step bunching, confirming that small QDs only require a step edge (more generally a defect) to nucleate [27]. Such different behaviour between small and large QDs is a further indication of their different origins.

3. Surface mass transport in the InAs/GaAs 2D–3D transition

3.1. Evidence by AFM volume analysis

One of the puzzling aspects of the self-assembled QDs is that the nucleated 3D volume is far larger than that being deposited in the narrow coverage range where the entire nucleation

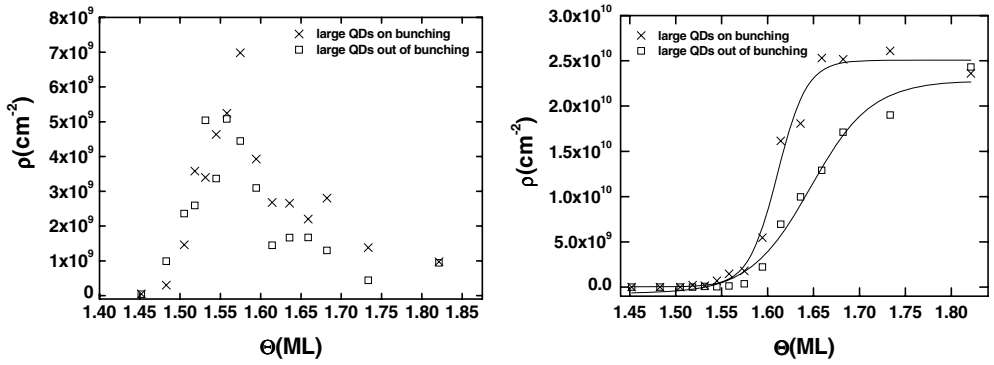

Figure 7. Number density dependence on InAs coverage of small and large QDs.

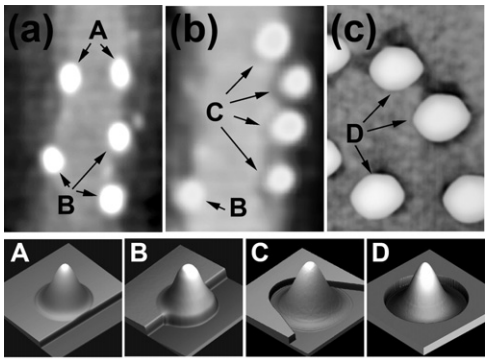

Figure 8. 120 × 160 nm^2 AFM images for coverages of 1.54 ML (a) and 1.61 ML (b). 'A' are QDs nucleated over the step edge, 'B' are QDs that have partially eroded the step edge, and 'C' QDs that have completely eroded it. (c) 80 × 120 nm^2 AFM image showing plane erosion occurring for 2.4 ML InAs growth at 522 °C ('D' are QDs after erosion). The bottom panels show schematic 3D views of QDs before and after the step or plane erosion.

process is completed. We discuss here a peculiar feature, recently discovered [31], at the origin of this phenomenon, which is associated with mature 3D QDs, i.e. the erosion of the step edge surrounding dots. This is clearly shown in figure 8, which compares two areas of the surface of InAs, with coverage 1.54 ML (panel (a)) and 1.61 ML (panel (b)), where the average volume of the 3D QDs amounts to ∼220 and ∼340 nm^3, respectively. QDs are observed nucleating preferentially at the upper side of step edges, as shown in panel (a). Comparing images for successive coverages one observes that QDs close to the step edge (A in panel (a)) progressively erode the step edge (B) until they appear detached (C in panel (b)), as shown in pictures A–D below the topographies. Such erosion is evident for dots over the step edges but is unclear for dots nucleated on flat areas of the surface. Nevertheless, signs of erosion of the surface plane surrounding dots (QDs labelled 'D' in panel (c)) were observed for growths at higher temperature (522 °C) and coverages (2.4 ML). In the last case the larger size of the dot (average volume ∼1500 nm^3) and, consequently, the larger strain energy at its base could explain the erosion. However, even at 500 °C a reduced plane erosion cannot be excluded because of the finite tip resolution.

As for other systems [32–35], substrate erosion may be favoured in this case by the In–Ga intermixing which draws material from the substrate to create the alloyed island. This

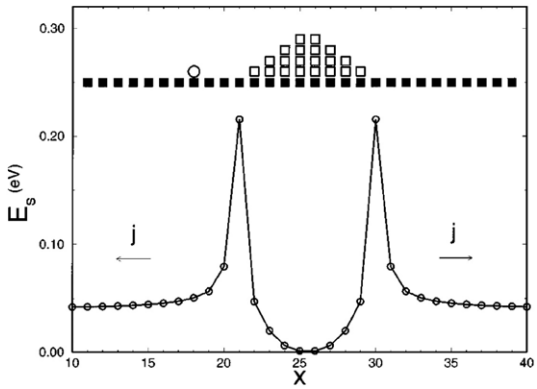

Figure 9. The strain energy around a typical island. The substrate (filled □) is shown in the upper part of the figure. E_s is the strain energy of an atom placed on the top of the substrate or on the island. Reused with permission from [37]. Copyright 1997, American Institute of Physics.

interpretation is supported by the work of Cullis *et al* [1] on $In_xGa_{1-x}As/GaAs$. This work predicts for $x = 1$ the largest elastic energy per atom and the highest In concentration in the upper layers of the QDs [1, 2, 36]. Around the QD, a compressive strained area forms where the elastic energy differs (see figure 9) from that of the WL far from the island by an amount that is large and positive; inside the dot, instead, it is negative [37, 38]. The minimum value is due to the partial strain relaxation inside the dot; the maximum, at the periphery, is due to the strain propagation along the interface, which increases the misfit between the underlying substrate and the WL around islands. We speculate that, because of the strain profile encircling QDs, the detachment rate of adatoms from steps is higher than the attachment rate, favouring the consumption of the step around dots.

In figure 10 the total dot volume is plotted as a function of the evaporated In amount. As in other studies [12, 14, 39, 40], figure 10 highlights the increase of the dot volume in the 2D–3D transition region for CG, GI and GI-flat samples. This increase is well beyond the volume of the material being deposited (straight line in the figure). Two regions with different slopes can be distinguished: in the range 1.6–1.8 ML, the dependence of the dot volume on coverage is linear, with slope $F_t \sim 4F_0$ for all the samples, where F_0 is the slope of the straight line representing the volume being deposited by the impinging InAs flux. Above 1.8 ML, the volume increases at the same rate F_0 as the coverage.

It is worth underlining that the volume behaviour just described is clear evidence of large surface mass transport from the 2D to the 3D phase at the very initial stage of the transition. This can be quantified as an extra coverage of approximately $\Delta\theta = 0.9$ ML for the CG and GI samples, and $\Delta\theta = 0.5$ ML for the GI-flat. Such mass transfer ends above 1.8 ML, above which the volume increase is solely at the expense of the incoming flux.

The ensuing discussion concerns the microscopic origin of such excess volume. The AFM topographies allow for a lower estimate of the amount of eroded material around islands. For the GI sample the fraction p of QDs placed below a step edge is plotted in the upper panel of figure 11 as a function of deposition. While at the beginning of nucleation all dots nucleate on a step edge (as dots A in figure 8(a)), at 1.9 ML ∼60% of them are found below it (as C in figure 8(b)). This is consistent with the fact that dots first nucleate at the upper side of the step edge, then, as a result of step erosion, they are located at the lower side of the step. The volume eroded from the steps, shown in the lower panel of figure 11, is approximately

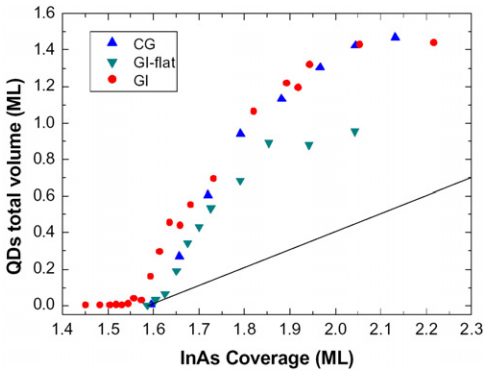

Figure 10. QDs volume plotted as a function of InAs coverage for the CG, GI and GI-flat samples. The lowest straight curve indicates the InAs flux above the 2D–3D transition.

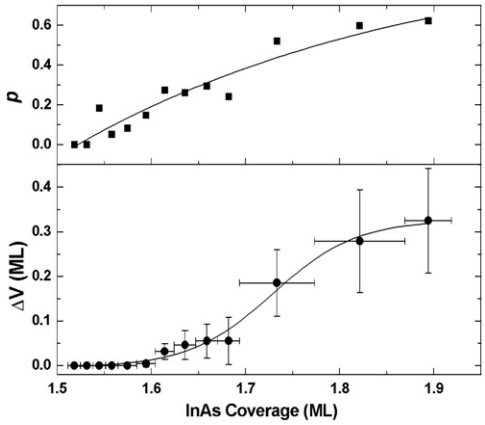

Figure 11. Upper panel: Fraction of QDs p below a step versus InAs coverage (GI sample). Lower panel: Volume ΔV drawn from the steps versus InAs coverage. The curves are guides for the eye.

$\Delta V = p\rho h \Delta S$, where ρ is the total QD density, ΔS is the area drawn from the step and h is the 1 ML step height. AFM measurements performed on several images give a value for ΔS not less than twice the mean basal area S of the QD. Considering that ΔS is somewhat larger than two and that we neglect the contribution of QDs placed across the step edge, the asymptotic value of $\Delta V = 0.3$ ML (figure 11) sets a lower limit to the surface mass current due to erosion. Therefore, in addition to surface segregation and substrate intermixing, a relevant fraction of the dot volume comes from step erosion: not enough, however, to account for all the 3D volume in excess if we just take into account the results reported in figure 11. A further contribution can be attributed to the presence of floating In adatoms at the very beginning of nucleation [20, 41].

In fact, STM images of a recent paper [42] indicate that a higher eroded volume is possible. A good input comes from the comparison of the total QD volume in the CG, GI and GI-flat samples, shown in figure 10. While for the CG and GI samples the excess volume $\Delta\theta_{\mathrm{CG}}$, $\Delta\theta_{\mathrm{GI}} \approx 0.9$ ML, for the GI-flat $\Delta\theta_{\mathrm{GI\text{-}flat}} \approx 0.5$ ML, thus suggesting an erosion dependence by the initial wetting layer morphology. This finding is still more interesting if compared with the step density per unit area for all the samples analysed. Just before the

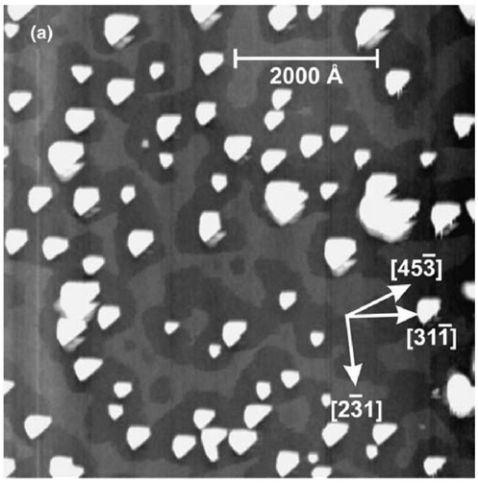

Figure 12. Overview STM image with InAs QDs grown on nominal GaAs(2511)A (6700 × 6700 Å^2), $U = 2.5$ V, $I = 0.15$ nA, InAs thickness 5.25 Å grown at a sample temperature T. Reproduced with permission from Elsevier [43].

transition starts, the CG and GI surfaces present a value $\rho_{\text{steps}}^{\text{CG}} = \rho_{\text{steps}}^{GI} = 23\ \mu\text{m}^{-1}$, while that for the GI-flat is $\rho_{\text{steps}}^{\text{GI-flat}} = 15\ \mu\text{m}^{-1}$. The relation between the step density and the excess volume is thus apparent: in particular, if we notice that the ratio $\rho_{\text{steps}}^{\text{GI-flat}}/\rho_{\text{steps}}^{\text{CG}}$ is similar to $\Delta\theta_{\text{GI-flat}}/\Delta\theta_{\text{CG}}$ and that the step erosion occurs with the same intensity for each sample, we infer that the overall excess volume has probably to be accounted for by step erosion (and, in general, wetting layer erosion). Such an interpretation is also strengthened by the disappearance of 2D islands during the large QD density explosion, i.e. when the step erosion is operating. Further support for the step (and WL) erosion contribution in the excess volume comes from STM images (see figure 12) of InAs islands deposited onto nominal and vicinal (1.0° off) GaAs(2511)A surfaces [43]. The authors find a massive WL erosion and the InAs material taken out of it is enough to justify the QD excess volume.

3.2. Evidence by RHEED intensity analysis

In addition to the volume behaviour, the most striking experimental evidence of surface mass transport comes from RHEED intensity data. In figure 13 the RHEED spot intensity evolution as a function of the growing time is shown for ∼2 ML of InAs deposited in the GI mode, i.e. in cycles of 5 s spaced by 25 s of growth interruption. On approaching θ_c (see the first three cycles of figure 13), the RHEED intensity is constant during GI; this fact indicates no substantial changes either in As stoichiometry and morphology of the alloyed (2 × 3)–(4 × 3) WL [20, 44] resulting from the equilibrium of the dynamical processes of As incorporation–desorption and In–Ga detachment, migration and incorporation into different lattice sites. However, for a total delivery of 1.59 ML (330 s to 360 s in the timescale of figure 13) the large morphological change of the surface on formation of QDs begins; at the same time the RHEED intensity changes suddenly. The largest variation in the intensity, in figure 13, is measured within the first two cycles above the critical value θ_c for a total coverage of 1.75 ML; two equal jumps follow in the next two cycles, when the coverage reaches 1.88 ML; finally, the intensity saturates in the last two, corresponding to a total coverage of 2.03 ML.

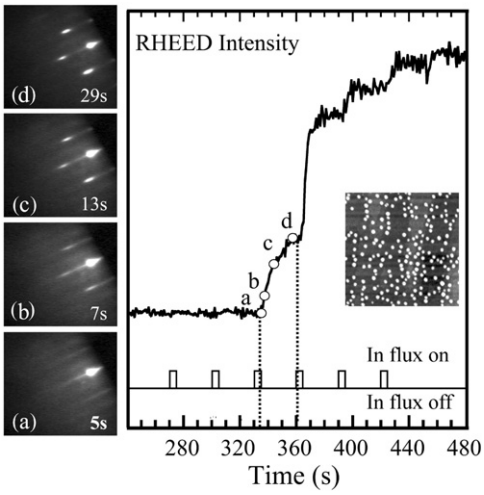

Figure 13. RHEED intensity of the (01) diffraction reflex as a function of time during the MBE-GI growth of InAs on GaAs(001). A total InAs coverage of 2.03 ML is delivered in consecutive cycles, each consisting of 5 s of In deposition followed by 25 s of growth interruption, while the As_4 cell shutter is always kept open. The left panels, (a) to (d), show the sequence of RHEED patterns observed at the specified times of the cycle (marked in the figure) where the total InAs coverage reaches 1.59 ± 0.01 ML. The 2D–3D transition occurs; meantime, no further In has been deposited on the surface. The inset shows a (600×600) nm^2 AFM image of the 3D QDs covering the surface, at the end of the growth.

The side patterns, shown in figures 13(a)–(d), refer to the time interval after the interruption of the In flux in the cycle corresponding to 1.59 ML of total In deposition. Remarkably, 3D spots start being observed ∼2 s after the GI. In fact, when the In shutter is closed, 5 s after the beginning of the cycle, the diffraction pattern is still like that observed in the preceding cycles, i.e. typical of a 2D surface with some degree of disorder; 3D spots appear about 2 s after the GI and are fully developed after 25 s. During the GI the In (Ga) content of the sample is constant, since any In (Ga) desorption, at 500 °C, is prevented by the high As flux, as also confirmed by the constant RHEED intensity during GI in the cycles preceding the 2D–3D transition [45]. Therefore, we can conclude that the RHEED intensity variations observed during the GI, at InAs thickness larger than 1.59 ML, are solely due to the increase of diffraction volume because of the large nucleation of QDs occurring on the timescale set by the processes of As desorption and cation (mainly In) surface diffusion.

To support this issue, we reported in figure 14 the QD number density versus InAs coverage for a sample grown, by MBE-GI, compared with RHEED pattern intensity of spotty features. The RHEED intensity data points reported in figure 14 are derived from figure 13 by assigning to the final coverage reached in each cycle (after 5 s of In evaporation) the intensity measured at the end of that cycle (after 25 s of GI). It is apparent that the RHEED changes closely follow the QD number density changes with coverage. Both start at about 1.59 ML, rapidly increase within 0.2 ML, and then saturate at approximately 2 ML, as expected, since each QD, independently of its size, contributes to diffraction only with a small fraction of its volume at the top. Hence, one can conclude that 3D nuclei are mostly formed within 0.2 ML from θ_c, their growth being triggered by the large surface diffusion of cations which is set up at this thickness.

It is interesting to compare the transition evolution for GI and CG samples. In the two sets of samples there is a substantial difference in the absolute values of the intensity at equal

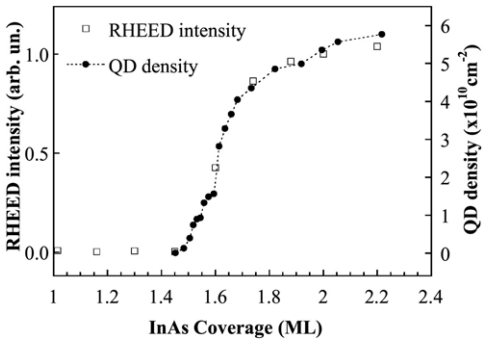

Figure 14. Open squares: RHEED intensity of the (01) diffraction reflex as a function of InAs MLs deposited on GaAs(001) by MBE-GI, i.e. by consecutive cycles consisting in 5 s of InAs growth followed by 25 s of growth interruption, leaving the As_4 cell shutter open. The data points are obtained from figure 13, by assigning the RHEED intensity measured at the end of each 30 s cycle to the total InAs coverage reached in that cycle. Filled dots: measured QD number density as a function of the InAs coverage. The comparison is made by normalizing at 2 ML where both QD density and RHEED intensity saturate.

coverage and/or temperature; the final morphologies also differ greatly. However, as will be shown later, comparing GI and CG RHEED intensities for the same temperature, we found that the onset values were identical, irrespective of the very different kinetics involved in the two growth modes. The 3D volume increase in this narrow coverage range is far larger than the deposited volume.

4. Scaling behaviour of self-assembled QDs

The key point lies in understanding the transition process between 1.57 and 1.61 ML. The comparison of the number density of the two QD families rules out the possibility that the large QDs are merely the evolution of the small ones since the low density of the small QDs cannot account for the density evolution of the large ones. To gain insight into the nature of these two families we have analysed the scaling behaviour of their size distribution. Dynamic scaling was first introduced to describe 2D islanding and was substantiated by computer simulations [46–48] and experimental studies both in homo- [49, 50] and heteroepitaxial [51–53] growth. To be specific, in the framework of dynamic scaling, the size distribution function of the number density of islands at coverage Θ is given by

$$N_i(u) = \frac{\Theta}{\langle s \rangle^2} f_i(u), \tag{1}$$

where $u = s/\langle s \rangle$, $\langle s \rangle$ being the island average size and f_i is the scaling function that, according to Amar and Family [48], reads, for $i \geqslant 1$,

$$f_i(u) = C_i u^i \mathrm{e}^{-\mathrm{i}a_i u^{1/a_i}}. \tag{2}$$

C_i and a_i are constants [48] that fulfil the relations

$$\frac{\Gamma[(i+2)a_i]}{\Gamma[(i+1)a_i]} = (\mathrm{i}a_i)^{a_i}, \qquad C_i = \frac{(\mathrm{i}a_i)^{(i+1)a_i}}{a_i \Gamma[(i+1)a_i]}, \tag{3}$$

where $\Gamma(x)$ is the gamma function. Ebiko *et al* [54] were the first to show the applicability of equation (1) to 3D growth in semiconductor heterostructures, provided that s was interpreted as the volume of the islands. Dynamic scaling makes it possible to determine the dimension of

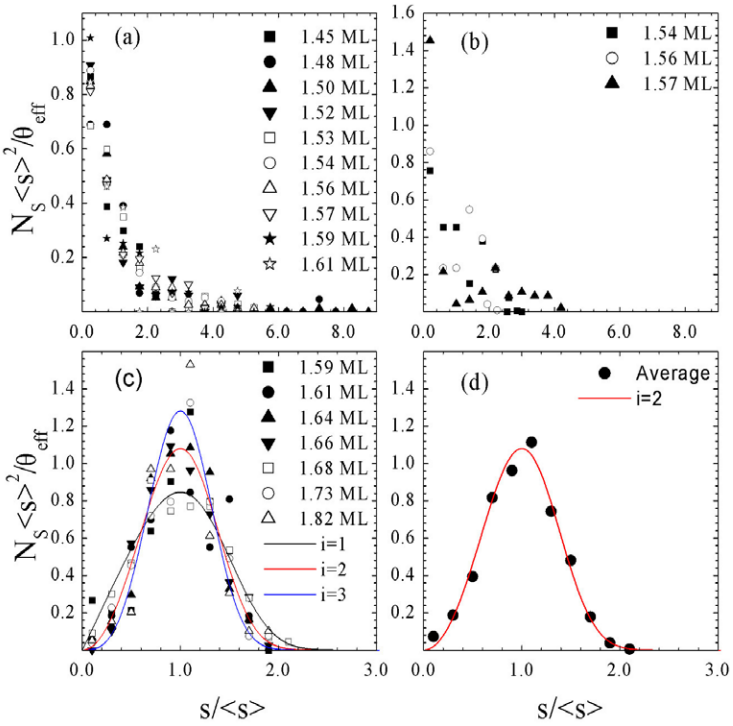

Figure 15. Scaled distributions of the experimental island volume of GI sample for small QDs (a), large QDs in the range 1.54–1.57 ML of InAs coverages (b) and large QDs in the range 1.59–1.82 ML of InAs coverages (c). Solid lines in panel (c) show the theoretical scaling function for $i = 1, 2, 3$. Panel (d) shows the average of the experimental distributions of panel (c) compared to the theoretical scaling function for $i = 2$.

the critical nucleus, i [46–48]. This is done by comparing the experimental size distribution of QDs and its evolution during the first stage of film formation to the theoretical function that, in turn, depends upon i. Figure 15 shows the scaled island volume distributions for the InAs deposits around the transition, from 1.45 to 1.82 ML. Both families have been included in the data analysis, taking care to separate the distributions related to the small and large QDs that are reported in figures 15(a), (b) and (c), respectively.

The scaling function for small QDs is featureless and nonzero for $s/\langle s\rangle \to 0$ [55]. It closely resembles that expected for a system with critical nucleus $i = 0$ [48, 56]. This implies that adatoms nucleate spontaneously on the surface. In fact, as noticed in section 3, such a behaviour can be explained by the presence of defects on the surface, such as steps: actually, small QDs nucleate almost exclusively at the upper edge of steps and 2D islands. This fact indicates the presence of a minimum in the potential in the proximity of the step edge that makes the diffusing monomer stable. The scaling function does not change between 1.45 and 1.61 ML; for higher coverages the small QD density is negligible with respect to that of large QDs.

As far as large QDs are concerned, we distinguish two different types of behaviour. Up to 1.57 ML of InAs deposit we find a transition region where large QDs' scaling function has not attained the final form yet (figure 15(c)). Starting from 1.59 ML (figure 15(a)) the size distributions change completely, approaching a bell shape. Figure 15(d) displays the

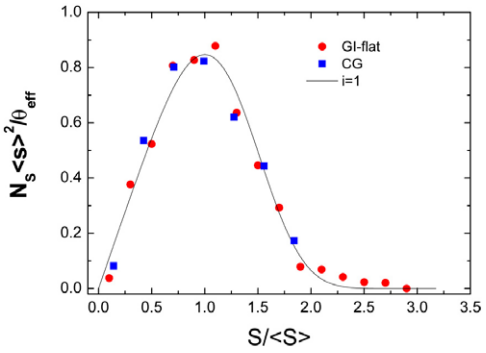

Figure 16. Averaged scaled distributions of the experimental island volume of CG (squares) and GI-flat (dots) samples. The solid line shows the theoretical scaling function for $i = 1$.

comparison between the $f_2(u)$ ($C_2 = 1.97$, $a_2 = 0.30$) function [48] and the averaged experimental data; the agreement between the two curves is excellent. The comparison between the scaling function for the small and large QDs suggests that two different aggregation mechanisms are operating and it allows us to maintain that large QDs are not merely the direct evolution of the small QDs.

Due to the growth mode used for the sample (25 s of growth interruption (GI) after every In evaporation cycle), ripening [57] cannot be excluded, which fact could affect our conclusions. Thus, to assess its significance, we have grown an analogous sample without growth interruptions. In this case, the scaling analysis for the small QDs (not shown) reveals the same result as for the GI sample. For the large QDs, there is still a bell-shaped scaling function compatible with $i = 1$ [54] as shown in figure 16. Therefore ripening, if any, does not affect the observed transition from a decaying to a bell shaped scaling function. Because of the complexity of the system under investigation, the model of Amar and Family could be oversimplified [48], particularly for the purpose of assigning the size of critical nuclei. The value of i can be employed all the same as a practical label for characterizing the scaling function and, in this case, for marking morphological transitions.

The origin of the transition between the two families of QDs can be understood if we consider the evolution, as a function of coverage, of the total volume contained in large QDs only. The total volume contained in large QDs is determined by the equation $V^T_{\text{large}} = \rho_{\text{large}}\langle V_{\text{large}}\rangle$, where ρ_{large} is the density of the large islands and $\langle V_{\text{large}}\rangle$ is the mean volume of the single large island. To specify how the variation of the large QD density and mean volume contribute to the volume increase of V^T_{large}, we plot separately in figure 17 the two terms $\frac{\mathrm{d}\rho_{\text{large}}}{\mathrm{d}\theta}\langle V_{\text{large}}\rangle$ and $\rho_{\text{large}}\frac{\mathrm{d}\langle V_{\text{large}}\rangle}{\mathrm{d}\theta}$ as a function of θ. The derivatives of ρ_{large} and $\langle V_{\text{large}}\rangle$ are calculated numerically by interpolating the experimental data. During the first stage of transition the volume increase is mainly due to the sudden nucleation of large islands and it is only subsequently that single island growth prevails. The conclusions are thus apparent: at the transition, the QD density explosion is triggered by the step erosion process [31, 42]; a great number of monomers becomes available, which allow for the explosive increase of the QD density at 1.6 ML (figures 5 and 17). At this stage the nucleation and growth are ruled by pure adatom diffusion.

The growth instability leading to the 2D–3D transition is thermodynamic in character, this being caused, as pointed out by Cullis *et al* [2], by the strain energy relaxation. Our data clearly show that the nucleation process begins at 1.45 ML of InAs deposition with the formation of

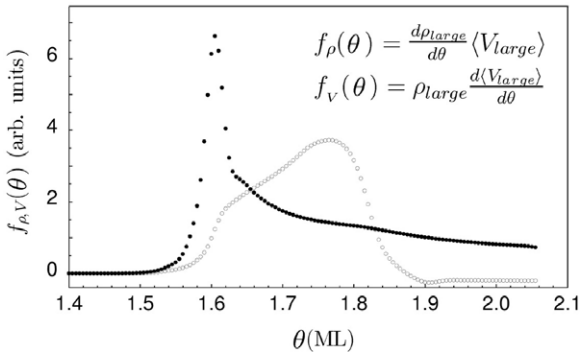

Figure 17. Derivative terms $\frac{\mathrm{d}\rho_{\mathrm{large}}}{\mathrm{d}\theta}\langle V_{\mathrm{large}}\rangle$ and $\rho_{\mathrm{large}}\frac{\mathrm{d}\langle V_{\mathrm{large}}\rangle}{\mathrm{d}\theta}$ of V^T_{large} plotted as a function of InAs coverage for the GI sample.

small nuclei at the step edges. In accordance with the model proposed by Dehaese *et al* [17], at 1.45 ML the average concentration of In in the uppermost layer is certainly larger than 82% [14]. Although the system, from a thermodynamic point of view, prefers growing by forming 3D islands, the conditions for this to occur are met at step edges first.

From the results of the scaling analysis we propose the following scenario: at 1.45 ML, heterogeneous nucleation begins because of the steps; the related scaling function is shown in figure 15(a). When the islands are large enough to trigger step erosion, a high additional concentration of diffusing monomers becomes available. The nucleation which follows always takes place at defects but, due to the large amount of diffusing material, the nuclei soon reach the critical size, giving rise to further erosion. In order to prove that at this stage the nucleation and growth of QDs is diffusion limited, we have studied the correlation between the volume distribution of QDs and the related area distribution of the cells of Voronoi tessellation [60]. Indeed, an excellent agreement has been found.

5. Temperature effects on the critical thickness

Experimental works report the shift of the 2D–3D transition to higher InAs deposition times for substrate temperatures above 500 °C. This shift is interpreted as an increase of the critical thickness due to the increased In intermixing with temperature [58]. In the following we will show that this shift does not really occur.

At the standard temperature of 500 °C the transition takes place at 1.59 ± 0.02 ML of InAs coverage. Two sets of samples have been grown for temperatures in the range between 455 and 560 °C: one set in the standard CG mode, and the other with growth interruptions (GI), as described in section 2.1. During growth interruptions of each cycle, the dynamical process of As absorption–desorption, more effective at step edges, allowed the cation atoms to detach themselves and migrate all over the surface toward more stable sites [59]. In InAs homoepitaxy the growth temperature of 500 °C is not usually exceeded so as to avoid possible In desorption for insufficient As_4 flux. In our case the flux ratio, As_4/In, was about 100 in order to prevent any In surface desorption [45].

In order to change the RHEED intensity measured as a function of time in the RHEED intensity as a function of InAs coverage, we measured the InAs growth velocity in the whole temperature range, as reported in table 1 of section 2.1.

The decrease of V_{InAs}, at constant beam fluxes, implies a diminished number of In adatoms on the surface, per unit time. This could be due to a decreased In sticking coefficient [61] or to

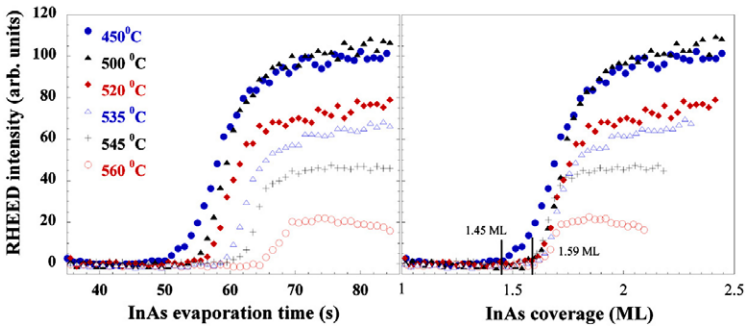

Figure 18. RHEED intensity for the set of InAs/GaAs samples grown at different temperatures in the continuous MBE mode, CG, as a function of the InAs evaporation time (left panel), and as a function of the InAs coverage in MLs, calculated by the effective growth fraction given by the inset in the right panel. The two onsets for formation of 'small' QDs, at 1.45 ML, and 'large' QDs, at 1.59 ML, are indicated. The former is clearly visible at low temperatures; the latter is commonly assumed as critical thickness for the 2D–3D transition.

an increased intermixing. However, a greater intermixing due to In–Ga exchange would affect the surface composition of the alloy but not its growth rate since the number of surface cations would not change. The latter one is, in fact, the only parameter which determines the growth velocity in III–V epitaxy.

The RHEED intensities during growth of CG samples are shown in figure 18 as a function of the InAs evaporation time (left panel), and as a function of the MLs of InAs coverage (right panel) calculated using the growth rates of table 1. The onset of the 2D–3D transition is delayed in time at increasing temperatures. Remarkably, however, such an onset does occur at the same critical thickness, up to 560 °C. Actually, two slope changes can be distinguished in the curves: a smaller one at 1.45 ML and a steeper one at 1.59 ML, both well defined at 450 °C. At higher temperatures the 1.45 ML edge becomes progressively less well defined while the one at 1.59 ML remains abrupt.

The same phenomenology is found if samples are grown by MBE with GI, i.e., by depositing InAs with periodic growth interruptions. Notice that growth interruptions would enhance the process of In bulk diffusion, if this is the case, compared to continuous growth. Figure 19 reports, in the left panel, the RHEED intensities at different temperatures, as a function of the time elapsed from the beginning of the growth. Like CG samples, the 2D–3D onset is delayed at increasing temperatures. The middle and right panels of figure 19 compare the intensities of CG and GI samples at 450 and 560 °C, respectively, as a function of the In evaporation time.

Thus, at odds with the current belief, temperature affects marginally the In–Ga intermixing and, accordingly, the surface and interface stress [62]. The observed shift in time of the 2D–3D onset is only due to the In sticking coefficient which is a rapidly decreasing function of temperature in the 450–560 °C range [58].

6. Conclusions

We have reported evidence of step erosion from QDs nucleated on step edges. Such an effect occurs, during the 2D–3D transition, in a narrow range of InAs coverage (1.6–1.8 ML) coincident with the sudden increase of QD density. The total QD volume growth rate is ∼4 times the impinging flux rate in the 1.6–1.8 ML range, and the same as the flux rate above

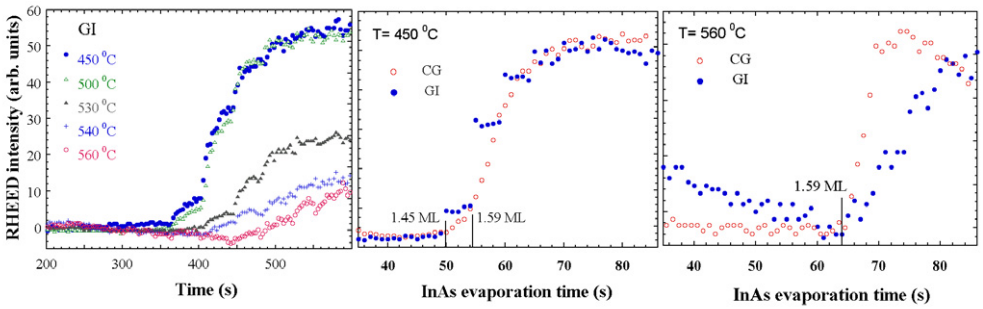

Figure 19. RHEED intensities, as a function of the time elapsed from the beginning of the growth (left panel), for the set of InAs/GaAs samples grown by MBE with growth interruptions, GI, at the specified temperatures. Each growth cycle consists of 5 s of In evaporation followed by 35 of growth interruption while the As_4 flux is continuously impinging on the surface. Middle and right panels show the comparison between CG and GI of the RHEED intensities at low and high temperatures as a function of the InAs evaporation time. For GI samples, only the RHEED intensity measured in the 5 s of In evaporation of each cycle is reported. Vertical scaling of CG and GI intensities is arbitrary, to emphasize threshold comparison.

1.9 ML. Thus, our data show that all processes involving the WL take place in a narrow range of coverages just above the S–K transition, after which no further contributions are observed. We also found evidence that the excess QD volume is linked to the step density of the WL, suggesting that it could be related to the step erosion.

The surface mass transport responsible for most of the nucleated volume of three-dimensional InAs QDs on GaAs(001) within a few tenths of a monolayer at the critical thickness has been evidenced by observing the 2D to 3D RHEED pattern transition during growth interruption. It is speculated that the cation current is triggered by the As desorption and by the lowering of the binding energy of In atoms due to compressive strain of the substrate at the critical composition. Such a condition is first met at θ_c around large dots sitting on step edges. In atom intermixing and segregation processes have a crucial role in InAs/GaAs(001) heteroepitaxy, because they determine the critical surface composition that triggers the 2D–3D growth instability. Such processes could be at the basis of an energetic mechanism that triggers the formation of quantum dots in strained heteroepitaxy. The critical thickness at which this formation occurs in the InAs/GaAs(001) system is quite independent of temperature in the range of 450–560 °C. Two thresholds are clearly distinguishable for the 2D–3D transition at temperatures below 500 °C: the first threshold occurs at 1.45 ML, where a low density of small islands nucleates at the upper step edges; the second is at 1.59 ML, where an explosive nucleation of 3D QDs takes place supported by the large surface mass current also due to the step erosion. Step instability and surface mass transport strongly influence the kinetic of the 2D–3D transition in InAs/GaAs [63]. Finally, using scaling arguments, we have highlighted the fact that, once the appropriate In concentration is reached, $i = 0$ nucleation is favoured thanks to steps. The subsequent step erosion produces a great number of fresh monomers, which, in turn, increase the probability of having the $i = 2$ (or, more generally, $i \neq 0$) nucleation over the entire surface.

Acknowledgments

Help in AFM measurements and analysis by V Sessi is gratefully acknowledged. The present work has been partially supported by the FIRB project RBNE01FSWY_007.

References

[1] Cullis A G, Norris D J, Walther T, Migliorato M A and Hopkinson M 2002 *Phys. Rev.* B **66** 081305
[2] Walther T, Cullis A G, Norris D J and Hopkinson M 2001 *Phys. Rev. Lett.* **86** 2381
[3] Cullis A G, Norris D J, Migliorato M A and Hopkinson M 2005 *Appl. Surf. Sci.* **244** 65
[4] Michler P, Kiraz A, Becher C, Schoenfeld W V, Petroff P M, Zhang L, Hu E and Imamoglu A 2000 *Science* **290** 2282
[5] Bonadeo N H, Erland J, Gammon D, Park D, Katzer D S and Steel D G 1998 *Science* **282** 1473
[6] Li X Q, Wu Y W, Steel D, Gammon D, Stievater T H, Katzer D S, Park D, Piermarocchi C and Sham L J 2003 *Science* **301** 809
[7] Bayer M, Hawrylak P, Hinzer K, Fafard S, Korkusinski M, Wasilewski Z R, Stern O and Forchel A 2001 *Science* **291** 451
[8] Stangl J, Holy V and Bauer G 2004 *Rev. Mod. Phys.* **76** 725 and references therein
[9] Joyce B A and Vvedensky D D 2004 *Mater. Sci. Eng.* R **46** 127 and references therein
[10] Leonard D, Pond K and Petroff P M 1994 *Phys. Rev.* B **50** 11687
[11] Kobayashi N P, Ramachandran T R, Chen P and Madhukar A 1996 *Appl. Phys. Lett.* **68** 3299
[12] Ramachandran T R, Heitz R, Chen P and Madhukar A 1996 *Appl. Phys. Lett.* **70** 640
[13] Krzyzewski T J, Joyce P B, Bell G R and Jones T S 2002 *Phys. Rev.* B **66** 121307(R)
[14] Patella F, Sgarlata A, Arciprete F, Nufris S, Skutznik P D, Placidi E, Fanfoni M, Motta N and Balzarotti A 2004 *J. Phys.: Condens. Matter* **16** S1503
[15] Ding Z, Bullock D W, Thibado P M, LaBella V P and Mullen K 2003 *Phys. Rev. Lett.* **90** 216109
[16] Moison J M, Guille C, Houzay F, Barthe F and Van Rompay M 1989 *Phys. Rev.* B **40** 6149
[17] Dehaese O, Wallart X and Mollot F 1995 *Appl. Phys. Lett.* **66** 52
[18] Fukatsu S, Fujita K, Yaguchi H, Shiraki Y and Ito R 1991 *Appl. Phys. Lett.* **59** 2103
[19] Tu Y and Tersoff J 2005 *Phys. Rev. Lett.* **93** 216101
[20] Patella F, Nufris S, Arciprete F, Fanfoni M, Placidi E, Sgarlata A and Balzarotti A 2003 *Phys. Rev.* B **67** 205308
[21] Da Silva M J, Quivy A A, Gonzàlez-Borrero P P, Marega E Jr and Leite J R 2002 *J. Cryst. Growth* **241** 19
[22] Costantini G, Rastelli A, Manzano C, Acosta-Diaz P, Katsaros G, Songmuang R, Schmidt O G, Känel O V and Kern K 2005 *J. Cryst. Growth* **278** 38
[23] Patella F, Arciprete F, Placidi E, Nufris S, Fanfoni M, Sgarlata A, Schiumarini D and Balzarotti A 2002 *Appl. Phys. Lett.* **81** 2270
[24] Schwoebel R L and Shipsey E J 1966 *J. Appl. Phys.* **37** 3682
[25] Kandel D and Weeks J D 1994 *Phys. Rev.* B **49** 5554
[26] Leon R, Senden T J, Kim Y, Jagadish C and Clark A 1997 *Phys. Rev. Lett.* **78** 4942
[27] Tsukamoto S, Honma T, Bell G R, Ishii A and Arakawa Y 2006 *Small* **2** 386
[28] Venables J A 1973 *Phil. Mag.* **27** 693
[29] Tomellini M and Fanfoni M 1997 *Chemistry for the 21st Century: Interfacial Science* ed M W Roberts (Oxford: Blackwell Science) chapter 6, p 6
[30] Krzyzewski T J, Joyce P B, Bell G R and Jones T S 2002 *Phys. Rev.* B **66** 201302(R)
[31] Placidi E, Arciprete F, Sessi V, Fanfoni M, Patella F and Balzarotti A 2005 *Appl. Phys. Lett.* **86** 241913
[32] Seifert W, Carlsson N, Johansson J, Pistol M and Samuelson L 1997 *J. Cryst. Growth* **170** 39
[33] Liao X Z, Zou J, Cockayne D J H, Jiang Z M, Wang X and Leon R 2000 *Appl. Phys. Lett.* **77** 1304
[34] Chaparro S A, Zhang Y and Drucker J 2000 *Appl. Phys. Lett.* **76** 3534
[35] Motta N 2002 *J. Phys.: Condens. Matter* **14** 8353 and references therein
[36] Kegel I, Metzger T H, Lorke A, Peisl J, Stangl J, Bauer G, Garcia J M and Petroff P M 2000 *Phys. Rev. Lett.* **85** 1694
[37] Barabàsi A L 1997 *Appl. Phys. Lett.* **70** 2565
[38] Le Goues F K, Reuter M C, Tersoff J, Hammar M and Tromp R M 1994 *Phys. Rev. Lett.* **73** 300
[39] Patella F, Fanfoni M, Arciprete F, Nufris S, Placidi E and Balzarotti A 2001 *Appl. Phys. Lett.* **78** 320
[40] Joyce P B, Krzyzewski T J, Bell G R, Joyce B A and Jones T S 1998 *Phys. Rev.* B **58** R15981
[41] Tsuyoshi H, Tsukamoto S and Arakawa Y 2006 *Japan. J. Appl. Phys.* **45** L777
[42] Xu M C, Temko Y, Suzuki T and Jacobi K 2005 *Surf. Sci.* **589** 91
[43] Temko Y, Suzuki T, Xu M C and Jacobi K 2005 *Surf. Sci.* **591** 117
[44] Mirecki Millunchick J, Riposan A, Dall B J, Pearson B and Orr B J 2003 *Appl. Phys. Lett.* **83** 1361
[45] Ohtake A and Ozeki M 2001 *Appl. Phys. Lett.* **78** 431
[46] Bartelt M C and Evans J W 1992 *Phys. Rev.* B **46** 12675
[47] Vicsek T and Family F 1984 *Phys. Rev. Lett.* **52** 1669
[48] Amar J G and Family F 1995 *Phys. Rev. Lett.* **74** 2066

[49] Stroscio J A and Pierce D T 1994 *Phys. Rev.* B **49** R8522
[50] Avery A R, Dobbs H T, Holmes D M, Joyce B A and Vvendesky D D 1997 *Phys. Rev. Lett.* **79** 3938
[51] Bressler-Hill V, Varma S, Lorke A, Nosho B Z, Petroff P M and Weinberg W H 1995 *Phys. Rev. Lett.* **74** 3209
[52] Bell G R, Krzyzewski T J, Joyce P B and Jones T S 2000 *Phys. Rev.* B **61** R10551
[53] Krzyzewski T J, Joyce P B, Bell G R and Jones T S 2002 *Surf. Sci.* **517** 8
[54] Ebiko Y, Muto S, Suzuki D, Itoh S, Shiramine K, Haga T, Nakata Y and Yokoyama N 1998 *Phys. Rev. Lett.* **80** 2650
[55] Arciprete F, Placidi E, Sessi V, Fanfoni M, Patella F and Balzarotti A 2006 *Appl. Phys. Lett.* **89** 041904
[56] Chambliss D D and Johnson K E 1994 *Phys. Rev.* B **50** 5012
[57] Zhang Z and Lagally M G 1997 *Science* **276** 377
[58] Heyn C and Hansen W 2003 *J. Cryst. Growth* **251** 218
[59] Horikoshi Y, Kawashima M and Yamaguchi H 1988 *Japan. J. Appl. Phys.* **27** 169
[60] Fanfoni M, Placidi E, Arciprete F, Orsini E, Patella F and Balzarotti A 2006 *Phys. Rev. Lett.* Submitted (*Preprint* Cond-Mat/0610118)
[61] Patella F, Arciprete F, Placidi E, Fanfoni M and Balzarotti A 2006 *Appl. Phys. Lett.* **88** 161903
[62] Silveira J P, Garcia J M and Briones F 2001 *J. Cryst. Growth* **227** 995
[63] Patella F, Arciprete F, Placidi E, Fanfoni M, Sessi V and Balzarotti A 2005 *Appl. Phys. Lett.* **87** 252101